The winner-take-all mechanism for all-optical systems of pattern recognition and max-pooling operation

Yahui Zhang, Shuiying Xiang, Xingxing Guo, Aijun Wen, Yue Hao

***Abstract*—The winner-take-all (WTA) mechanism based on the inhibitory dynamics of vertical-cavity surface-emitting laser with an embedded saturable absorber (VCSEL-SA) neurons is proposed for the first time. The WTA mechanism is shown numerically in a photonic spiking neural network (SNN). The effect of bias current on WTA time window is analyzed based on the proposed SNN. Moreover, a pattern recognition approach is presented numerically based on the WTA mechanism in all-optical neural network consisting of VCSEL-SA neurons. For the pattern recognition, the robustness of noisy inputs is examined. The effects of bias current, strength of inhibition and weight matrix on the speed of pattern recognition are analyzed carefully. Furthermore, the max-pooling operation is implemented numerically in the all-optical VCSEL-SA neural network model based on the WTA mechanism for the first time. The results hold great promise for the development of energy-efficient and high-speed photonic spiking neural network.**

***Index Terms*—vertical-cavity surface-emitting lasers, winner-take-all mechanism, pattern recognition system, max-pooling system.**

I. Introduction

In neuromorphic systems, pattern recognition concerns the description or classification of patterns. This capability is often a prerequisite for intelligent behavior and it is considered essential in tasks such as developing autonomous, intelligent computers, autonomous transportation, or even automated mail sorting [1-2]. Additionally, the convolutional neural networks (CNNs) can achieve superior performance on visual object recognition tasks. In CNNs, trainable filters and local neighborhood pooling operations are applied alternatingly on the raw input images [3]. Especially, when combined with max-pooling, the CNN has emerged as robust supervised feature learning and classification tool. Max-pooling operation leads to faster convergence rate by selecting superior invariant features that improve generalization performance [4]. For the pattern recognition and max-pooling operation, the winner-take-all (WTA) mechanism is a vital strategy, which allows only the most strongly-activated neuron in a group to respond with spiking activity [5-8]. Moreover, the WTA mechanism is widely applicable, including visual filters, competitive learning and decision-making tasks [9-13]. Compared with threshold gates and sigmoidal gates, WTA is a surprisingly powerful computational module [9].

Recently, pattern recognition, CNN and max-pooling operation have gained remarkable attention [14-27]. For instance, pattern recognition was achieved in the memristor neuromorphic systems [17, 18]. In 2018, the features of patterns were learnt in the spiking deep CNN that comprised the max-pooling layer [19]. Additionally, the spike pattern recognition was implemented on a multi-core embedded platform in 2018 [20]. In parallel, photonic neural network is a promising candidate for realizing hardware of pattern recognition, CNN and max-pooling operation due to energy efficiency and high-speed nature [15-16, 21-27]. For pattern recognition, in 2016, a simple pattern recognition task was achieved based on two cascaded excitable graphene fiber ring lasers [15, 16]. The neuromorphic photonic approach could potentially operate 6-8 orders of magnitude faster than neuromorphic electronics when accounting for the bandwidth reduction of virtualizing interconnects [15, 16]. The energy of per multiply-and-accumulate (MAC) operation based on the photonic hybrid platform is 1.3pJ [16]. In Neurogrid and HICANN, the energy of per MAC operation is 119pJ and 198.4pJ respectively [16]. In 2020, a pattern recognition was successfully demonstrated in vertical-cavity surface-emitting lasers (VCSELs) at GHz rates [27]. For CNN and max-pooling operation, a photonic CNN accelerator was proposed in 2018 to speed-up the convolution operation for CNNs. The system offers up to more than 3 orders of magnitude faster execution time and its optical core potentially offers more than 5 order of magnitude speed-up when compared to the state-of-the-art electronic counterparts [21]. In 2019, a complete digital electronic and analog photonic architecture capable of performing highly efficient CNNs for image recognition was presented, which comprises the max-pooling operation. The system

Manuscript received Oct 14, 2019. This work is supported in part by the National Natural Science Foundation of China (61674119, 61974177); National Postdoctoral Program For innovative Talents in China (BX201600118); Young Talent fund of University Association for Science and Technology in Shaanxi, China (20160109); Natural Science Basic Research Plan in Shaanxi Province of China (2017JM6002, 2016JM6009); Postdoctoral Science Foundation in Shaanxi Province of China; Fundamental Research Funds for the Central Universities and the Innovation Fund of Xidian University (5001-20109195456).

S. Xiang is with State Key Laboratory of Integrated Service Networks, Xidian University, Xi'an 710071, China; and also with State Key Discipline Laboratory of Wide Bandgap Semiconductor Technology, School of Microelectronics, Xidian University, Xi'an 710071, China (email: jxxsy@126.com).

Y. Zhang, X. Guo, A. Wen are with State Key Laboratory of Integrated Service Networks, Xidian University, Xi'an 710071, China.

Y. Hao is with State Key Discipline Laboratory of Wide Bandgap Semiconductor Technology, School of Microelectronics, Xidian University, Xi'an 710071, China

has potential to be 2.8 to 14 times faster while maintaining the same power usage of current state-of-the-art GPUs [25]. However, for pattern recognition, the reported networks were limited to recognize either specific patterns or the first spike time of patterns. In general, it is difficult to classify the patterns in the simple all-optical neural network. For CNN, the all-optical max-pooling operation, which can be incorporated into an all-optical CNN, is highly desirable for enhancing the convergence rate and the robustness of CNN.

VCSELs are already extensively used in photonic neural networks, as they offer many advantages including a variety of neuron-like characteristics, low manufacturing cost and energy-efficiency [28-32]. Here, VCSELs with an embedded saturable absorber (VCSELs-SA) are used as photonic neurons in the SNN.

In this paper, we propose for the first time the WTA mechanism based on the inhibitory dynamics of VCSELs-SA neurons. The WTA mechanism is shown numerically in the photonic SNN. Moreover, the pattern recognition and max-pooling operation are presented in the all-optical SNN based on the WTA mechanism. To the best of our knowledge, it is the first numerical implementation of photonic WTA mechanism based on VCSELs-SA as well as all-optical max-pooling operation. The rest of this paper is organized as follows. In Section II, the proposed photonic SNN system architecture for WTA mechanism is described. In addition, the theoretical model of VCSEL-based photonic neuron is presented. In Section III, the WTA mechanism is presented in the all-optical neural network. The pattern recognition is also presented in detail. Furthermore, for the pattern recognition, the robustness to noisy inputs is examined. The effects of bias current, strength of inhibition and weight matrix on the speed of pattern recognition are analyzed. Finally, the max-pooling operation is realized in the all-optical brain-inspired network that utilizes the WTA mechanism. Finally, conclusions are drawn in Section IV.

II. THEORY AND MODEL

The schematic diagram for WTA mechanism is presented in Fig. 1. Light coming from the tunable laser (TL) is conveyed through a modulator (Mod). A pulse signal generator (PPG) is used for creating the different pulse patterns required to perform measurements. The polarization state of the modulated light can be adjusted by the polarization controller (PC1). The injected strength of the modulated light is easily controlled by the variable optical attenuator (VOA_1). The modulated light is injected into the X-polarization (XP) mode of $VCSEL_M$-SA through the optical circulator (OC_1). The XP mode output of $VCSEL_M$-SA is separated by the polarizing beam splitter (PBS_1). The information from PPG is encoded into spikes by the photonic neuron ($VCSEL_M$-SA) in the XP mode [32]. Then, the XP mode output of $VCSEL_M$-SA is divided into two parts by means of (50/50) fiber couple (FC_1). The first optical branch is connected to $VCSEL_A$-SA through FC_2 and OC_2, and the strength is controlled by VOA_2. The second optical path is connected into the $VCSEL_B$-SA through FC_3 and OC_3, and the strength is controlled by VOA_3. The XP mode outputs of $VCSEL_A$-SA and $VCSEL_B$-SA are also divided into two branches. One XP output path of $VCSEL_A$-SA ($VCSEL_B$-SA) is connected to the Y-polarization (YP) mode of $VCSEL_B$-SA ($VCSEL_A$-SA) through PC3 (PC2). The other XP mode output branch is connected to the output ports ($output_1$ and $output_2$) where the signal is recorded. The two VCSELs-SA ($VCSEL_A$-SA and $VCSEL_B$-SA) as two neurons in this arrangement "compete" with each other. And the "winner" will make the response.

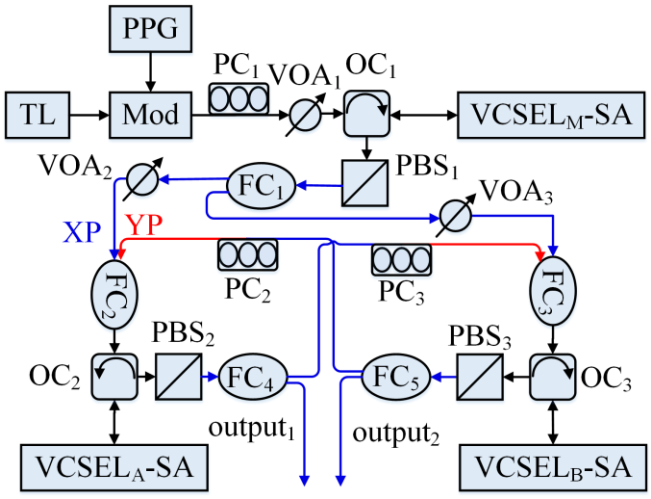

Fig. 1. Schematic diagram of WTA based on two VCSELs-SA. TL: tunable laser; PPG: pulse signal generator; Mod: modulator; PC: polarization controller; VOA: variable optical attenuator; FC: fiber couple; OC: optical circulator; VCSEL-SA: vertical-cavity surface-emitting laser with an embedded saturable absorber; PBS: polarization beam splitter; Blue line: XP mode; Red line: YP mode.

Here, the theoretical model of VCSELs-SA, is considered as the combination of spin-flip and Yamada models [32, 33]. For simplicity, the model of $VCSEL_M$-SA, which is an encoding neuron, is not shown. In the models of $VCSEL_A$-SA and $VCSEL_B$-SA, the variables F denote the slowly varying complex amplitudes. D are the total carrier inversions between the conduction and valence bands related to the transparency carrier density. d describe the carrier inversions with opposite spin orientations. The rate equations for F, D and d can be written as follows [32, 33]:

$$\begin{aligned}\dot{F}_x^{A,B} =& \frac{1}{2}(1+i\alpha^{A,B})[(D_1^{A,B}+D_2^{A,B}-1)F_x^{A,B}+i(d_1^{A,B}+d_2^{A,B})F_y^{A,B}] \\ &-(\varepsilon_a^{A,B}+i\varepsilon_p^{A,B})F_x^{A,B}+\sqrt{\beta_{sp}^{A,B}}\xi_x^{A,B} \\ &+k_{MA,MB}F_x^{M}(t-\tau_{MA,MB})e^{-i\omega_x^{M}\tau_{MA,MB}+i\Delta\omega_x^{MA,MB}t}\end{aligned} \quad (1)$$

$$\begin{aligned}\dot{F}_y^{A,B} =& \frac{1}{2}(1+i\alpha^{A,B})[(D_1^{A,B}+D_2^{A,B}-1)F_y^{A,B}-i(d_1^{A,B}+d_2^{A,B})F_x^{A,B}] \\ &+(\varepsilon_a^{A,B}+i\varepsilon_p^{A,B})F_y^{A,B}+\sqrt{\beta_{sp}^{A,B}}\xi_y^{A,B} \\ &+k_{BA,AB}F_x^{B,A}(t-\tau_{BA,AB})e^{-i\omega_x^{B,A}\tau_{BA,AB}+i\Delta\omega_x^{BA,AB}t}\end{aligned} \quad (2)$$

$$\begin{aligned}\dot{D}_{1,2}^{A,B} =& \gamma_{1,2}^{A,B}[\mu_{1,2}^{A,B}-D_{1,2}^{A,B}-\frac{1}{2}a_{1,2}^{A,B}(D_{1,2}^{A,B}+d_{1,2}^{A,B})\left|F_x^{A,B}-iF_y^{A,B}\right|^2 \\ &-\frac{1}{2}a_{1,2}^{A,B}(D_{1,2}^{A,B}-d_{1,2}^{A,B})\left|F_x^{A,B}+iF_y^{A,B}\right|^2+c_{12,21}^{A,B}D_{2,1}^{A,B}]\end{aligned} \quad (3)$$

$$\begin{aligned}\dot{d}_{1,2}^{A,B} =& -\gamma_{s1,2}^{A,B}d_{1,2}^{A,B}-\gamma_{1,2}^{A,B}[\frac{1}{2}a_{1,2}^{A,B}(D_{1,2}^{A,B}+d_{1,2}^{A,B})\left|F_x^{A,B}-iF_y^{A,B}\right|^2 \\ &-\frac{1}{2}a_{1,2}^{A,B}(D_{1,2}^{A,B}-d_{1,2}^{A,B})\left|F_x^{A,B}+iF_y^{A,B}\right|^2-c_{12,21}^{A,B}d_{2,1}^{A,B}]\end{aligned} \quad (4)$$

where superscripts M, A and B represent $VCSEL_M$-SA

TABLE I
SOME PARAMETERS OF VCSELS-SA USED IN SIMULATION [32, 33]

Symbol	Description	Value
γ_1	Total carrier decay rates in pump region	1.09×10^{-3}
γ_2	Total carrier decay rates in absorbing region	1.13×10^{-3}
γ_{s1}	Effective spin-flip rates in pump region	0.25
γ_{s2}	Effective spin-flip rates in absorbing region	0.25
μ_1	Injected current in pump region	2.1
μ_2	Injected current in absorbing region	-6.1
a_1	Differential gain in pump region	1
a_2	Differential gain in absorbing region	8.7
α	Linewidth enhancement factor	3
κ	Cavity decay rate	$390ns^{-1}$
γ_p	Birefringence	$15ns^{-1}$
ε_a	Amplitude anisotropy	0
c_{12}	Carrier diffusion rate from pump region to absorbing region	2.84×10^{-2}
c_{21}	Carrier diffusion rate from absorbing region to pump region	1.91
ε_p	Phase anisotropy	γ_p/κ
β_{sp}	Strength of spontaneous emission	10^{-5}

$VCSEL_A$-SA and $VCSEL_B$-SA, respectively. Subscripts x and y represent the XP and YP modes, respectively. Subscripts 1 and 2 are the pump and absorbing regions, respectively. The terms $k_{MA,MB}F_x^M(t-\tau_{MA,MB})e^{-i\omega_x^M\tau_{MA,MB}+i\Delta\omega_x^{MA,MB}t}$ in Eq. (1) represent the injections from $VCSEL_M$-SA to the XP modes of $VCSEL_A$-SA and $VCSEL_B$-SA, where $k_{MA,MB}$ are connection weights, $F_x^M(t-\tau_{MA,MB})$ characterize the shapes of injections, $\tau_{MA,MB}$ are time delays from $VCSEL_M$-SA to $VCSEL_A$-SA and from $VCSEL_M$-SA to $VCSEL_B$-SA, $\Delta\omega_x^{MA,MB}$ are the angular frequency detuning between the injecting field and the $VCSEL_{A,B}$-SA. The terms $k_{BA,AB}F_x^{B,A}(t-\tau_{BA,AB})e^{-i\omega_x^{B,A}\tau_{BA,AB}+i\Delta\omega_x^{BA,AB}t}$ in Eq. (2) describe the injections from the XP modes of $VCSEL_B$-SA and $VCSEL_A$-SA into the YP modes of $VCSEL_A$-SA and $VCSEL_B$-SA with the coupling strengths $k_{BA,AB}$ and coupling delays $\tau_{BA,AB}$. The terms $\sqrt{\beta_{sp}^{A,B}}\xi_x^{A,B}$ and $\sqrt{\beta_{sp}^{A,B}}\xi_y^{A,B}$ are the Gaussian white noise in the XP and YP modes of the VCESLs-SA, where $\xi_x^{A,B}$ and $\xi_y^{A,B}$ are independent Gaussian white noise sources with zero mean and unit variance. The terms $c_{12}^{A,B}D_2^{A,B}$ and $c_{21}^{A,B}D_1^{A,B}$ are the carrier diffusions. Here, we define $\varepsilon_p^{A,B}=\gamma_p^{A,B}/\kappa^{A,B}$. The equations are written in a dimensionless form such that the time is measured in the units of $(\kappa^{A,B})^{-1}$. The rest of parameters, which are the same for $VCSEL_A$-SA and $VCSEL_B$-SA, are presented in Table I. The analytically calculated and the simulated lasing current threshold μ_{1th} of VCSELs-SA is about 2.5 [32]. With these parameters, the VCSELs-SA without any external optical injection operate below the lasing threshold. Thus, no laser light is emitted for the free running VCSELs-SA.

III. NUMERICAL RESULTS

In this section, we first show the WTA mechanism in the proposed photonic SNN. The effect of bias current on WTA time window is analyzed. Following that, the WTA mechanism is used in the all-optical pattern recognition system. For the pattern recognition, the robustness of the system is examined. The effects of bias current, strength of inhibition and weight matrix on the speed of pattern recognition are analyzed. Finally, the WTA mechanism is incorporated into the max-pooling operation system.

Based on the proposed photonic SNN and model of VCSELs-SA, we define the intensities as $I_x=|F_x|^2$, $I_y=|F_y|^2$. The connection weights are k_{MA} =0.23, k_{MB} =0.23. The delay times are τ_{MA} =7ns and τ_{MB} = 8ns. We assume that the information is represented by the rectangular pulse with 5ns duration time and 0.5 injected strength. The simulated results of three VCSELs-SA in Fig. 1 for WTA mechanism are presented in Fig. 2. For one case, in left panel of Fig. 2, the rectangular pulse is encoded into one spike by $VCSEL_M$-SA in Fig. 2(a1) [32]. The amplitude of the spike is 156.6. Then, the spike that generated in Fig. 2(a1) is injected into both $VCSEL_A$-SA and $VCSEL_B$-SA. It can be seen from Figs. 2(a2) and (a3), with $k_{BA}=k_{AB}=0$, spikes are generated by both $VCSEL_A$-SA and $VCSEL_B$-SA. For different case, in right panel of Fig. 2, with the same rectangular pulse, one spike is also generated by $VCSEL_M$-SA (in Fig. 2(b1)). Differently, in Figs. 2(b2) -(b3), with $k_{BA}=k_{AB}=0.25$, a spike is only generated by $VCSEL_A$-SA. Thus, $VCSEL_A$-SA is the winner due to a smaller delay time. This is due to the fact that spike generated by $VCSEL_A$-SA is injected into the YP mode of $VCSEL_B$-SA. A spike is generated in the YP mode of $VCSEL_B$-SA [32]. And the spike from $VCSEL_M$-SA cannot fire a spike in the XP mode due to refractory period of $VCSEL_B$-SA [34]. This response demonstrates the WTA mechanism in the proposed photonic SNN. It also can be found that the WTA mechanism is mainly dependent on the lateral inhibition of photonic neuron [32]. When the complete lateral inhibition appears, the WTA mechanism is realized.

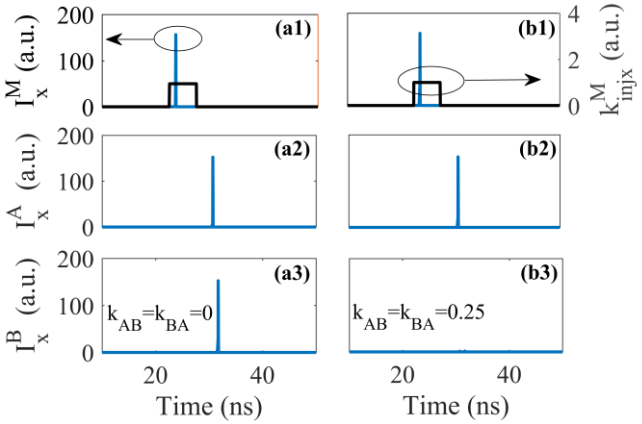

Fig. 2 The injection of $VCSEL_M$-SA and the outputs of $VCSEL_{M,A,B}$-SA for WTA mechanism. (a1) -(a3): $k_{BA}=k_{AB}=0$, (b1) -(b3): $k_{BA}=k_{AB}=0.25$.

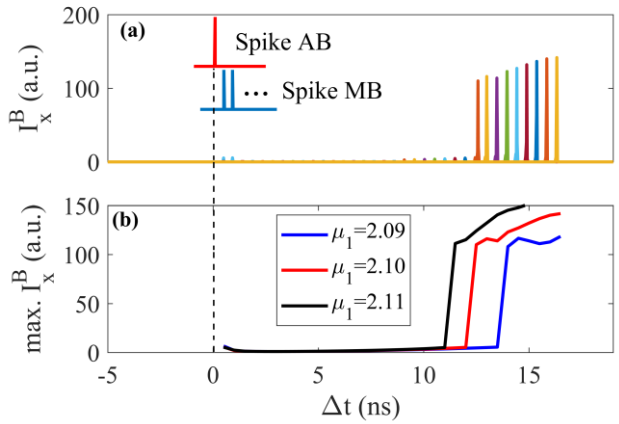

Fig. 3 (a) The excited spikes as functions of Δt in the XP mode of $VCSEL_B$-SA. (b) The amplitudes of spikes as functions of Δt in the XP mode with different μ_1.

To investigate time windows of the WTA mechanism based on the inhibitory dynamics of photonic neurons, the outputs of $VCSEL_B$-SA neuron for different injected spikes are presented in Fig. 3. Here, we assume that $\tau_{MA} < \tau_{MB}$, $VCSEL_A$-SA is a winner. The relative time delay difference between two optical patches of $VCSEL_M$-SA is defined as $\Delta t=\tau_{MB}-\tau_{MA}$. Here, to compare directly, we ignore the delay time from $VCSEL_A$-SA to $VCSEL_B$-SA. The connection weights are $k_{AB}=0.25$, k_{MB}=0.23. The XP mode outputs of $VCSEL_B$-SA as functions of Δt are presented in Fig. 3(a). The inset of Fig. 3(a) illustrates the relationship between Spike AB and Spike MB. The Spike AB (MB) is the spike from $VCSEL_A$-SA ($VCSEL_M$-SA) to $VCSEL_B$-SA. For simplicity, we consider that an excited spike is generated when the maximum amplitude of the spike is higher than 20. It can be seen that there is no elicited spike with Δt <12.5ns. Thus, the WTA mechanism is realized in the photonic neuron with the time window Δt <12.5ns. Moreover, the maximum intensities of excited spikes as functions of Δt with different μ_1 are presented in Fig. 3(b). It indicates that the WTA time window is wider with a smaller μ_1. More precisely, the WTA time windows are 14ns, 12.5ns and 11.5ns with μ_1 =2.09, 2.10 and 2.11, respectively.

Next, we consider the all-optical SNN for pattern recognition based on the WTA mechanism. The schematic diagram of the pattern recognition neural network equipped with the WTA mechanism is presented in Fig. 4. The fully connected neural network consists of two presynaptic neurons ($VCSEL\text{-}SA_1$ and $VCSEL\text{-}SA_2$) and two postsynaptic neurons ($VCSEL\text{-}SA_3$ and $VCSEL\text{-}SA_4$). Here, $W_{13}=W_{24}=W_1$ =0.23, $W_{14}=W_{23}=W_2$ = 0.01. The time delays between the presynaptic neurons and postsynaptic neurons are selected as 7ns. Between postsynaptic neurons, the output of the XP mode is injected into the YP mode of the other postsynaptic neuron. The connection between postsynaptic neurons is similar to the connection between $VCSEL_A$-SA and $VCSEL_B$-SA in Fig. 1. The connection weight between two postsynaptic neurons is defined as k_{wy}. Here, the information is represented by the spatial temporal pattern. The different patterns are distinguished by spatial relationship and temporal relationship between different pulses. For example, in Fig. 4, the spatial and temporal relationships of two rectangular pulses (the orange rectangular pulse ahead of the black rectangular pulse; the orange rectangular pulse is injected into $VCSEL_1$-SA, the black rectangular pulse is injected into $VCSEL_2$-SA) consist a pattern which can be defined as Pattern 1. The spatial and temporal relationships of another two rectangular pulses (the orange rectangular pulse lags the black rectangular pulse; the orange rectangular pulse is injected into $VCSEL_1$-SA, the black rectangular pulse is injected into $VCSEL_2$-SA) represent another pattern which can be defined as Pattern 2. Rectangular pulses can also be encoded into spikes that have the same spatial and temporal relationships in the XP mode of presynaptic neurons. The pattern that consists by spikes (orange spike and black spike) in Fig. 4 is also called Patten 1.

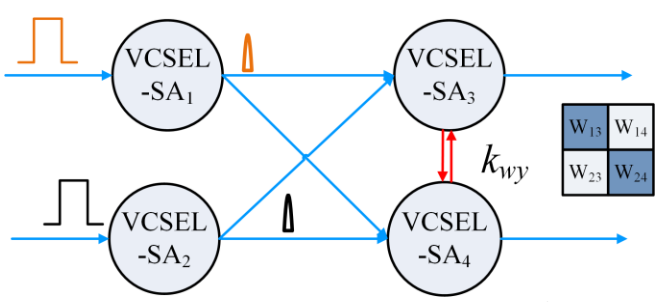

Fig. 4 The photonic SNN equipped with the WTA mechanism for pattern recognition.

Figures 5(a)-(d) show the responses of four VCSELs-SA for different signal-to-noise ratios (SNRs). Here, for Pattern 1 and Pattern 2, the time differences between two spikes of one pattern are ± 5ns, respectively. Figures 5(a)-(b) present the results of encoding. The rectangular pulses in Fig. 4 of pattern 1 are encoded into two spikes, which orange rectangular pulse injected into $VCSEL_1$-SA is encoded into a spike in Fig. 5(a) Pattern 1 circle, and blue rectangular pulse injected into $VCSEL_2$-SA is encoded into a spike in Fig. 5(b) Pattern 1 circle. The results of pattern recognition are presented in Figs. 5(c)-(d). It can be seen that, for Pattern 1, a spike is generated by

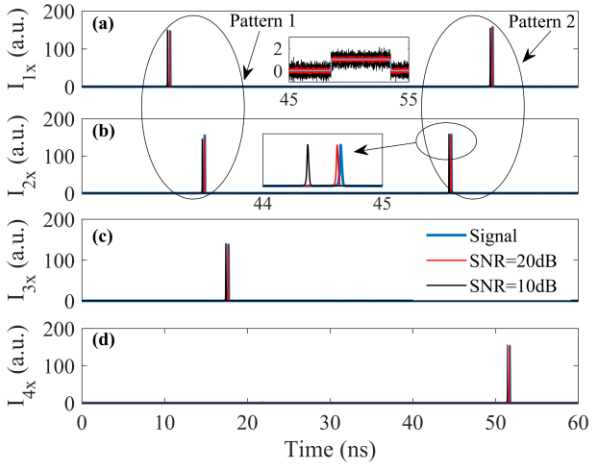

Fig. 5 (a)-(d) The responses of four VCSELs-SA with different SNRs injected rectangular pulses. The inset in (a) is the injected rectangular pulses with different SNRs. The inset in (b) indicates an enlargement of the generated spikes in Fig. 5(b).

VCSEL$_3$-SA in Fig. 5(c). For Pattern 2, a spike is generated by VCSEL$_4$-SA in Fig. 5(d). Patterns are recognized by spikes which are generated by VCSELs-SA. It is the pattern recognition based on the WTA mechanism. Without the WTA mechanism, both VCSEL$_3$-SA and VCSEL$_4$-SA generate spikes for Pattern 1 or Pattern 2. The inset in Fig. 5(a) shows the injected rectangular pulse without noise, with SNR=20dB and 10dB. The inset in Fig. 5(b) is an enlargement of spikes in Fig. 5(b). The spikes with different jitters are generated due to different SNRs. For patterns with jitter, the pattern recognition is also achieved in Figs. 5(c) and (d). That is to say, the neural system is robust to noisy injected pulses and spike jittering to some extent. Interestingly, we find when the first spike of the pattern is generated by VCSEL-SA$_1$ (VCSEL-SA$_2$), the winner neuron is VCSEL-SA$_3$ (VCSEL-SA$_4$) that generates a spike. That is to say, the first spike can be recognized in the proposed photonic SNN. Furthermore, the first spike of three-spikes pattern can also be recognized in the SNN based on the WTA mechanism.

We define the minimal time interval of two first spikes in two patterns for successful pattern recognition as ΔT_1. Figure 6(a) presents the ΔT_1 as functions of k_{wy} for different μ_1. It can be seen that, for a smaller μ_1, the minimum of k_{wy} leading to the successful pattern recognition is larger. With other k_{wy} less than the minimum, the pattern recognition cannot be achieved. More precisely, the minimum of k_{wy} for successful pattern recognition are k_{wy} =0.24, 0.19 and 0.16 for μ_1 =2.08, 2.10 and 2.12. Besides, for a larger μ_1, the ΔT_1 is smaller with the same k_{wy}. For instance, when k_{wy} =0.3, ΔT_1 =12ns, 9.2ns and 7.8ns for μ_1 =2.08, 2.10 and 2.12, respectively. That is to say, the speed of recognition ($1/\Delta T_1$) became faster with a larger μ_1 and k_{wy} to some extent. Two-dimensional map of ΔT_1 in the parameter space of W_1 and W_2 is shown in Fig. 6(b). It indicates that, when 0.22< W_1 <0.41, W_2 <0.07, the neural system can recognize the pattern. Besides, with the increase of W_1, ΔT_1 is decreased to some extent. When W_2 >0.2, the system cannot recognize the patterns. That is to say, a larger W_1 and a smaller W_2 are needed for a higher speed of pattern recognition.

Next, we incorporate the WTA mechanism into the max-pooling operation. The schematic diagram of max-pooling operation is presented in Fig. 7(a). The size of the input image

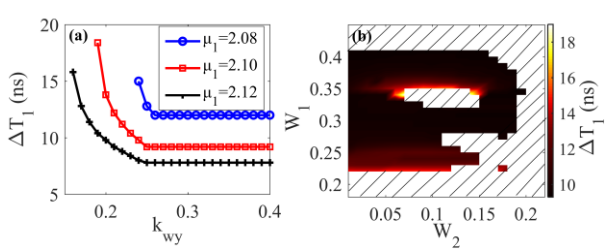

Fig. 6 (a) ΔT_1 as functions of k_{wy} for different μ_1. (b) Two-dimensional map of ΔT_1 in parameter space of W_1 and W_2.

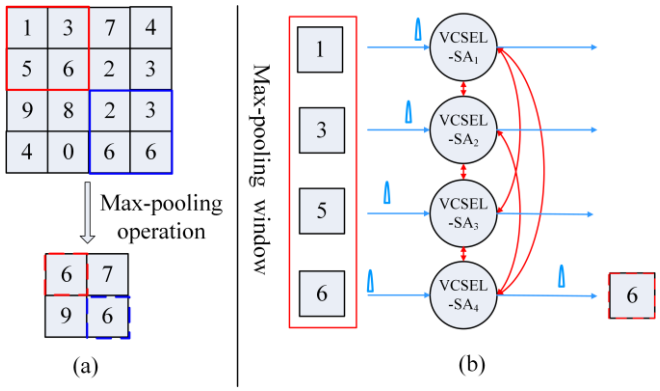

Fig. 7 (a) The schematic diagram of max-pooling operation. (b) The schematic diagram of SNN for max-pooling operation. The red and blue solid boxes are two max-pooling windows. The red (blue) dashed box is the max-pooling result of the red (blue) solid box. One square represents one pixel.

is considered as 4×4. The window of max-pooling is considered as 2×2 (red solid box in Fig. 7(a)). We set the moving pixels to be two in one axis (x or y) for sampling max-pooling operation. The value in each pixel represents the activity level. Such max-pooling operation determines the maximum value pixel in the max-pooling window. In case there are multiple pixels with equal maximal value in the max-pooling window, the earlier maximum value pixel is selected. For example, the pixel of value 6 (red dashed box) is selected among the pixels of values 1, 3, 5 and 6 (max-pooling window). The third pixel with value 6 is selected among the pixels of values 2, 3, 6 and 6 (blue box). The schematic diagram of all-optical neural system for max-pooling operation is presented in Fig. 7(b). The connection among four VCSELs-SA is same to the connection between VCSEL$_A$-SA and VCSEL$_B$-SA in Fig. 1. For example, the XP mode output of VCSEL$_1$-SA is injected into the YP mode of VCSEL$_2$-SA, VCSEL$_3$-SA and VCSEL$_4$-SA. The value of each pixel is encoded by the spatial temporal spike. Here, the reversed time coding is used in temporal spikes. The time interval of two adjacent value is set as 1.2ns. To select the first maximum value pixel, the spiking timings with same value and different pixels are set different. The difference of two adjacent pixel spike timing is set as 0.3ns with the same pixel value. For example, value 5 of the third pixel is encoded at 29ns, value 5 of the fourth pixel is encoded at 29.3ns, value 6 of fourth pixel thus is encoded at 28.1ns. Each spatial temporal spike that represents each pixel is injected into the XP mode of each VCSEL-SA, respectively.

The simulation of max-pooling operation is depicted in Fig.

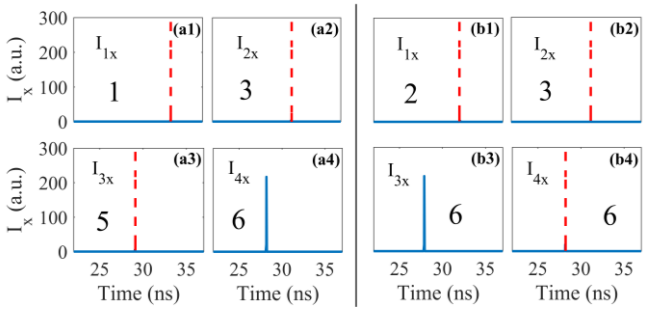

Fig. 8 The responses of four VCSELs-SA for max-pooling. (a1)-(a4) red box in Fig. 7. (b1)-(b4) blue box in Fig.7.

8. For the red box max-pooling window in Fig. 7(a), the spikes represented values 1, 3, 5 and 6 are injected into the XP modes of $VCSEL_1$-SA at 33.2ns, $VCSEL_2$-SA at 31.1ns, $VCSEL_3$-SA at 29.0ns and $VCSEL_4$-SA at 28.1ns, respectively. Figures 8(a1)-(a4) represent the responses of the XP mode of four VCSELs-SA. It can be seen that only VCSEL-SA_4 generates the spike with 28.1ns, which represents value 6 pixel. Thus, the max-pooling operation is realized based on the WTA mechanism. With two maximum value pixels, the example (blue box in Fig. 7(a)) of max-pooling operation is presented in Figs. 8(b1) - (b4). The spikes represented values 6 of third pixel and 6 of fourth pixel are injected into the XP modes of $VCSEL_3$-SA at 27.8ns and $VCSEL_4$-SA at 28.1ns, respectively. The spike only generated in VCSEL-SA_3 with 27.8, which shows that in such situation, the first maximum value pixel is selected. In the other two max-pooling windows (in Fig. 7(a)), the results of max-pooling operation are also realized. The pixels of values 7 and 9 are selected.

IV. Conclusion

In present work, we realize the WTA mechanism based on the inhibitory dynamics of VCSELs-SA neurons for the first time. The time window of WTA mechanism is wider with a smaller bias current. In addition, the photonic WTA mechanism is used in all-optical spiking pattern recognition. In spiking pattern recognition, the system is robust to noise. The speed of recognition is faster with a larger bias current and strength of inhibition to some extent. Additionally, the max-pooling operation is realized in an all-optical neural network based on the WTA mechanism. To the best of our knowledge, such WTA mechanism based on the inhibitory dynamics of VCSELs-SA neurons has not yet been reported. These findings are valuable for realizing decision-making tasks in brain-inspired photonic neuromorphic systems. Furthermore, all-optical neural network equipped with WTA mechanism holds promise for the development of all-optical fast pattern recognition systems. Moreover, the all-optical max-pooling operation offers great potentials for the improvement of efficiency and performance in all-optical CNN.

Acknowledgment

We would like to thank Dr. Matěj Hejda, from University of Strathclyde, for helpful writing advice and the proofreading of the manuscript.

References

[1]. R. J. Schalkoff, "Pattern recognition," in *Wiley Encyclopedia of Computer Science and Engineering*, B.Wah, Ed. Dec. 2007.

[2]. A. K. Jain, R. P. W. Duin and J. Mao, "Statistical pattern recognition: A review," *IEEE T. Pattern Anal.*, vol. 22, no. 1, pp. 4–37, Jan. 2000.

[3]. S. Ji, W. Xu, M. Yang and K. Yu, "3D convolutional neural networks for human action recognition," *IEEE T. Pattern Anal.*, vol. 35, no. 1, pp. 221-231, Jan. 2013.

[4]. J. Nagi, F. Ducatelle,G. A. D. Caro,and D. Ciresan, "Max-pooling convolutional neural networks for vision-based hand gesture recognition," *IEEE ICSIP*, Kuala Lumpur, Malaysia, Nov. 2011.

[5]. R. Coultrip, R. Granger and G. Lynch, "A cortical model of winner-take-all competition via lateral inhibition," *Neural Netw.*, vol. 5, no. 1, pp. 47-54, 1992.

[6]. A. J. Yu, M. A. Giese and T. A. Poggio, "Biophysiologically plausible implementations of the maximum operation," *Neural Comput.*, vol. 14, no. 12, pp.2857-2881, Dec. 2002.

[7]. G. A. Rousselet, S. J. Thorpe and M. Fabre-Thorpe, "Taking the MAX from neuronal responses," *Trends Cogn. Sci.* vol. 7, no. 3 pp. 99–102, Mar. 2003.

[8]. K. M. Cherry and L. Qian, "Scaling up molecular pattern recognition with DNA-based winner-take-all neural networks," *Nature*, vol. 559, no. 7714, pp. 370-376, 2018.

[9]. W. Maass, "On the computational power of winner-take-all," *Neural Comput.*, vol.12, no.11, pp. 2519-2535, Nov. 2000.

[10]. D. K. Lee, L. Itti, C. Koch and J. Braun, "Attention activates winner-take-all competition among visual filters," *Nat. Neurosci.*, vol. 2, no. 4, pp. 375-381, Apr. 1999.

[11]. A. Roxin and A. Ledberg, "Neurobiological models of two-choice decision making aan Bbe reduced to a one-dimensional nonlinear diffusion equation," *Plos. Comput. Biol.*, vol. 4, no. 3, Mar. 2008, Art. no: e1000046.

[12]. A. Gupta and L. N. Long, "Hebbian learning with winner take all for spiking neural networks," *IEEE International Joint Conference on Neural Networks*, pp. 1054-1060, Atlanta, GA, USA, Jun. 2009.

[13]. N. Lynch, C. Musco and M. Parte, "Winner-take-all computation in spiking neural networks," 2019 [Online] arXiv preprint arXiv:1904.12591.

[14]. M. A. Nahmias, B. J. Shastri, A. N. Tait and P. R. Prucnal, "A leaky integrate-and-fire laser neuron for ultrafast cognitive computing," *IEEE J. Sel. Top. Quantum Electron.*, vol.19, no. 5, pp. 1-12 Sept.-Oct. 2013.

[15]. B. J. Shastri, M. A. Nahmias, A. N. Tait, A. W. Rodriguez, B. Wu and P. R. Prucnal, "Spike processing with a graphene excitable laser," *Sci. Rep.*, vol. 6, no.1, pp. 1-12, Jan. 2016.

[16]. T. F. De Lima, B. J. Shastri, A. N. Tait, M. A. Nahmias and P. R. Prucnal, "Progress in neuromorphic photonics," *Nanophotonics*, vol. 6, no. 3, pp. 577-599, Mar. 2017.

[17]. Y. Zhang, Y. Li, X. Wang and E. G. Friedman, "Synaptic characteristics of Ag/AgInSbTe/Ta-based memristor for pattern recognition applications," *IEEE T. Electron Dev.*, vol. 64, no. 4, pp. 1806-1811, Apr. 2017.

[18]. Y. Zhang, X. Wang and E. G. Friedman, "Memristor-based circuit design for multilayer neural networks," *IEEE T. Circuits-I*, vol. 65, no. 2, pp. 677-686, Feb. 2018.

[19]. S. R. Kheradpisheh, M. Ganjtabesh, S. J. Thorpe and T. Masquelier, "STDP-based spiking deep convolutional neural networks for object recognition," *Neural Netw.*, vol. 99, pp. 56-67, Mar. 2018.

[20]. F. Grassia, T. Levi, E. Doukkali and T. Kohno, "Spike pattern recognition using artificial neuron and Spike-Timing-Dependent Plasticity implemented on a multi-core embedded platform," *Artificial Life and Robotics*, vol. 23, no. 2, pp.200-204, Jun. 2018.

[21]. A. Mehrabian, Y. Al-Kabani, V. J. Sorger and T. El-Ghazawi, "PCNNA: A photonic convolutional neural network accelerator," In 2018 31st, IEEE ISOCC, pp.169-173, Arlington, VA, USA, Sept. 2018.

[22]. S. Xiang, Y. Zhang, J. Gong, X. Guo, L. Lin and Y. Hao, "STDP-based unsupervised spike pattern learning in a photonic spiking neural network with VCSELs and VCSOAs," *IEEE J. Sel. Top. Quantum Electron.*, vol.25, no. 6, pp.1-9, Nov.-Dec. 2019.

[23]. J. Feldmann, N. Youngblood, C. D. Wright, H. Bhaskaran and W. H. P. Pernice, "All-optical spiking neurosynaptic networks with self-learning capabilities," *Nature*, vol. 569, no.7755, pp. 208-214, May. 2019.

[24]. S. Xu, J. Wang, R. Wang, J. Chen and W. Zou, "High-accuracy optical convolution unit architecture for convolutional neural networks by cascaded acousto-optical modulator arrays," *Opt. Express*, vol. 27, no. 14, pp.19778-19787, Jul. 2019.

[25]. V. Bangari *et al.*, "Digital Electronics and Analog Photonics for Convolutional Neural Networks (DEAP-CNNs)," 2019, [online] arXiv preprint arXiv:1907.01525.

[26]. S. Y. Xiang, Z. Ren, Y. Zhang, Z. Song and Y. Hao, "All-optical neuromorphic XOR operation with inhibitory dynamics of a single photonic spiking neuron based on VCSEL-SA," *Opt. Lett.*, vol. 45, no. 5, pp. 1104-1107, Mar. 2020.

[27]. J. Robertson, M. Hejda, J. Bueno and A. Hurtado, "Ultrafast optical integration and pattern classification for neuromorphic photonics based on spiking VCSEL neurons," *Sci. Rep.*, vol.10, no. 1, pp. 1-8 Apr. 2020.

[28]. A. Hurtado, I. D. Henning and M. J. Adams, "Optical neuron using polarisation switching in a 1550nm-VCSEL," *Opt. Express*, vol. 18, no. 24, pp. 25170-25176, Nov. 2010.

[29]. A. Hurtado, K. Schires, I. D. Henning and M. J. Adams, "Investigation of vertical cavity surface emitting laser dynamics for neuromorphic photonic systems," *Appl. Phys. Lett.*, vol. 100, no.10, Mar. 2012, Art. no. 103703.
[30]. N. Li, H. Susanto, B. R. Cemlyn, I. D. Henning and M. J. Adams, "Stability and bifurcation analysis of spin-polarized vertical-cavity surface-emitting lasers," *Phys. Rev. A*, vol. 96, no. 1, Jul. 2017, Art. no. 013840.
[31]. Y. Zhang, S. Xiang, J. Gong, X. Guo, A. Wen and Y. Hao, "Spike encoding and storage properties in mutually coupled vertical-cavity surface-emitting lasers subject to optical pulse injection," *Appl. Optics*, vol. 57, no. 7, pp.1731-1737, Mar. 2018.
[32]. Y. Zhang, S. Xiang, X. Guo, A. Wen and Y. Hao, "All-optical inhibitory dynamics in photonic neuron based on polarization mode competition in a VCSEL with an embedded saturable absorber," *Opt. Lett.*, vol. 44, no. 7, pp. 1548-1551, Apr. 2019.
[33]. A. Scirè, J. Mulet, C. R. Mirasso and M. San Miguel, "Intensity and polarization self-pulsations in vertical-cavity surface-emitting lasers," *Opt. Lett*., vol. 27, no. 6, pp. 391-393, Mar. 2002.
[34]. F. Selmi, R. Braive, G. Beaudoin, I. Sagnes, R. Kuszelewicz, and S. Barbay, "Relative Refractory Period in an Excitable Semiconductor Laser," *Phy. Rev. Lett*, vol. 112, May 2014, Art. no. 183902.

Yahui Zhang was born in Hebei, China, in 1993. She is currently working toward the Ph.D. degree from Xidian University, Xi'an, China. Her researching interest is the vertical cavity surface-emitting lasers, neuromorphic photonic systems.

Shuiying Xiang was born in Jiangxi, China, in 1986. She received the Ph.D. degree from Southwest Jiaotong University, Chengdu, China, in 2013. She is currently a Professor with the State Key Laboratory of Integrated Service Networks, Xidian University, Xi'an, China. She is the author or coauthor of more than 100 research papers. Her research interests include neuromorphic photonic systems, brain-inspired information processing, spiking neural network, vertical cavity surface-emitting lasers, and semiconductor lasers dynamics.

Xingxing Guo was born in Jiangxi, China, in 1993. She is currently working toward the Ph.D. degree from Xidian University, Xi'an, China. Her researching interest is the dynamics and applications of semiconductor lasers.

Aijun Wen was born in Shannxi, China, in 1968. He received the Ph.D. degree from Xidian University, Xi'an, China, in 1998.

He is a Professor with State Key Laboratory of Integrated Service Networks, Xidian University, Xi'an, China. His current research interests include microwave photonics and optical communication.

Yue Hao was born in the city of Chongqing, China, in 1958. He received the Ph.D. degree from Xi'an Jiao tong University, Xi'an, China, in 1991.

He is currently a Professor at State Key Discipline Laboratory of Wide Bandgap Semiconductor Technology, the School of Microelectronics, Xidian University, Xi'an, China. His research interests include wide forbidden band semiconductor materials and devices.